Volume 15
Number 39
21 October 2024
Pages 15939–16394

Chemical Science

rsc.li/chemical-science

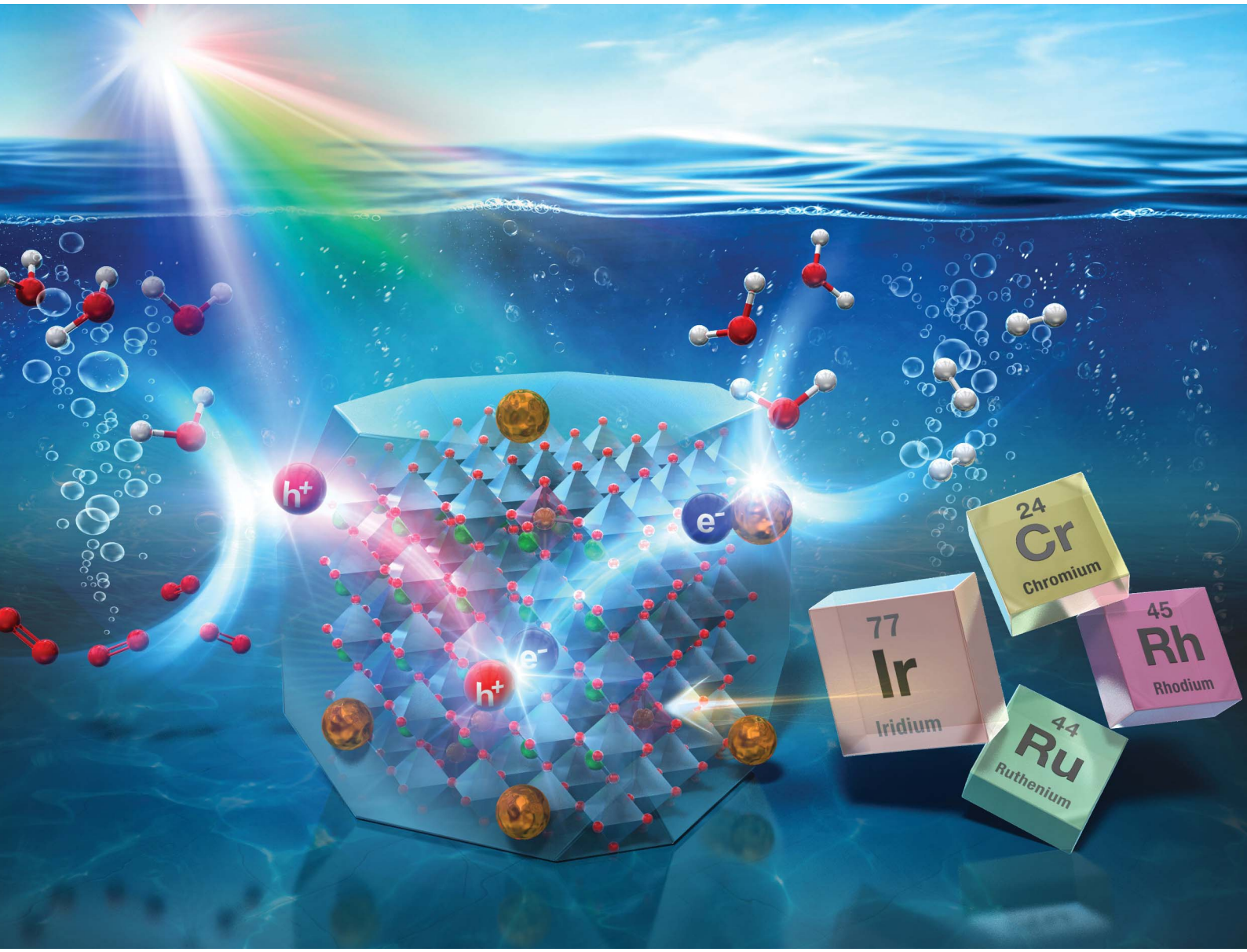

ISSN 2041-6539

ROYAL SOCIETY OF CHEMISTRY

EDGE ARTICLE

Akihiko Kudo *et al.*

Water splitting over transition metal-doped $SrTiO_3$ photocatalysts with response to visible light up to 660 nm

Chemical Science

ROYAL SOCIETY OF CHEMISTRY

EDGE ARTICLE

View Article Online
View Journal | View Issue

Cite this: *Chem. Sci.*, 2024, **15**, 16025

All publication charges for this article have been paid for by the Royal Society of Chemistry

Water splitting over transition metal-doped $SrTiO_3$ photocatalysts with response to visible light up to 660 nm†

Kyohei Kaiya,[a] Yoshiya Ueki,[a] Hiromasa Kawamoto,[a] Kenta Watanabe,[a] Shunya Yoshino,[a] Yuichi Yamaguchi[ab] and Akihiko Kudo*[ab]

Received 18th June 2024
Accepted 4th September 2024

DOI: 10.1039/d4sc03978e

rsc.li/chemical-science

Highly efficient water splitting under visible light irradiation was achieved using Ir, Sb, and Al-codoped $SrTiO_3$ of a single particulate metal oxide photocatalyst by a solid-state reaction followed by flux treatment using $SrCl_2$ and loading of a $RhCrO_x$ cocatalyst. The photocatalytic activity was improved by Al_2O_3 addition to the flux treatment, and doping of small amounts of Ir and Sb. It is notable that the water splitting over the photocatalyst proceeded with response to visible light up to 660 nm. This response wavelength is the longest compared with previously reported single particulate visible-light-driven photocatalysts for water splitting. The apparent quantum yield at 420 nm of the optimized photocatalyst was 0.73%. This photocatalyst was active for solar water splitting and gave 0.33% solar-to-hydrogen energy conversion efficiency (STH). Notably, water splitting proceeded giving 0.035% STH under visible light (λ > 440 nm) in a solar spectrum. Additionally, Rh, Ru, and Cr-doped $SrTiO_3$ photocatalysts were also successfully developed for highly efficient water splitting under visible light irradiation by application of the strategies of small amounts of doping, flux treatment with $SrCl_2$ with Al_2O_3 addition, and loading of a $RhCrO_x$ cocatalyst.

Introduction

Solar green hydrogen production by photocatalytic water splitting, which is an uphill reaction to convert sunlight energy into storable chemical energy, is a promising method to solve resource, energy, and environmental issues.[1–4] For practical use of this technology, a photocatalytic water splitting system employing powdered materials is attractive due to its simplicity and low-cost.[2,5,6] It is important to develop a visible light responsive powdered photocatalyst from the viewpoint of efficient utilization of solar light.

The photocatalytic water splitting system is classified into single particulate and Z-scheme systems.[2,7–10] The Z-scheme system consists of a H_2-evolving photocatalyst, an O_2-evolving photocatalyst, and an electron mediator. In contrast to it, a single particulate system has the great advantage of being a simple system. To achieve single particulate photocatalytic water splitting, it is necessary to develop a photocatalyst possessing thermodynamically satisfactory valence and conduction bands for the oxidation and reduction of water, respectively. Additionally, a narrow band gap is required for response to visible light. Therefore, development of a single particulate photocatalyst for efficient water splitting under visible light irradiation is a challenging topic.

(Oxy)nitrides and oxysulfides such as GaN–ZnO,[11,12] $ZnGeN_2$–ZnO,[13,14] $Y_2Ti_2O_5S_2$,[15] Ta_3N_5,[16] TaON,[17] $LaMg_{1/3}Ta_{2/3}O_2N$,[18] $BaTaO_2N$,[19,20] and $SrTaO_2N$[21] as single particulate photocatalysts have been developed for water splitting under visible light irradiation. The valence bands of these materials consist of hybridized N 2p–O 2p and S 3p–O 2p orbitals, resulting in a narrow band gap. However, these material groups sometimes suffer from self-oxidation by holes generated by light irradiation. In contrast, metal oxides are promising materials because many of them are chemically stable even under light irradiation. However, they often possess a wide band gap because of a deep valence band consisting of O 2p orbitals.

Doping of metal cations to host materials is a useful strategy for sensitization of metal oxides with a wide bandgap to visible light.[2,22–27] As an example, a single particulate Rh and Sb-codoped $SrTiO_3$ ($SrTiO_3$:Rh,Sb) photocatalyst split water under visible light irradiation.[28] The photocatalyst responded to visible light up to 500 nm for water splitting. Sb is doped as an Sb^{5+} ion to a Ti^{4+} site in a $SrTiO_3$ host, leading to the formation of a Rh^{3+} ion due to charge compensation. Sb codoping is a key issue because $SrTiO_3$:Rh without the Sb codoping showed no activity for water splitting. Recently, we have developed a $SrTiO_3$:Ir photocatalyst responding to the whole range of visible light up to 700 and 800 nm as O_2- and H_2-evolving photocatalysts in the presence of a sacrificial electron donor, respectively.[29,30] Thus, a $SrTiO_3$:Ir

[a]*Department of Applied Chemistry, Faculty of Science, Tokyo University of Science, Shinjuku-ku, Tokyo 162-8601, Japan. E-mail: a-kudo@rs.tus.ac.jp*

[b]*Carbon Value Research Center, Research Institute for Science and Technology, Tokyo University of Science, Noda-shi, Chiba-ken 278-8510, Japan*

† Electronic supplementary information (ESI) available: Flowchart, details of characterisation (XRF, SEM), and the activities for water splitting of the materials. See DOI: https://doi.org/10.1039/d4sc03978e

photocatalyst is expected to show activity for water splitting under visible light with a long wavelength.

In recent years, Domen and co-workers have reported that an Al-doped $SrTiO_3$ ($SrTiO_3$:Al) photocatalyst[31–33] loaded with Rh/Cr_2O_3 and CoOOH cocatalysts showed high activity for water splitting under UV light irradiation.[34] 95.9% apparent quantum yield (AQY) at *ca.* 360 nm was obtained, indicating that the photo-generated carriers could react with water with negligible recombination. The high activity was attributed to the formation of fine particles of *ca.* 300 nm with the surface facet for water reduction and oxidation by flux treatment and Al doping during the treatment.[34] Furthermore, loading of Rh/Cr_2O_3 and CoOOH cocatalysts which are highly active sites for the reduction and oxidation of water was also essential to achieve efficient water splitting. However, $SrTiO_3$:Al responds to only UV light because of its wide band gap. Therefore, sensitization of the photocatalyst to visible light is necessary.

In the present study, we have developed an Ir-doped $SrTiO_3$:Al photocatalyst prepared by optimization of doping amounts, flux treatment using $SrCl_2$ with/without Al_2O_3 addition as a dopant of Al, and a cocatalyst aiming at highly efficient water splitting under visible light irradiation. Additionally, we examined various transition metal-doped $SrTiO_3$:Al photocatalysts for water splitting under visible light irradiation.

Experimental

Preparation of photocatalysts

$SrTiO_3$:M(x%),Sb(y%) (M = Ir, Rh, Ru, Cr, Mn, Fe, Co, Ni) photocatalysts were synthesized by a solid-state reaction (SSR). The starting materials of $SrCO_3$ (Kanto Chemical; 99.9%), TiO_2 (Kojundo Chemical; 99.99%), IrO_2 (Kojundo Chemical), Rh_2O_3 (Fujifilm Wako Pure Chemical; 99.5%), RuO_2 (Fujifilm Wako Pure Chemical), Cr_2O_3 (Rare Metallic; 99.9%), MnO_2 (Fujifilm Wako Pure Chemical; 99.5%), Fe_2O_3 (Fujifilm Wako Pure Chemical; 99.0%), Co_3O_4 (Kojundo Chemical; 99.95%), NiO (Kanto Chemical; 99.9%) and Sb_2O_3 (Nacalai Tesque; 98%) were mixed in an alumina mortar with an atomic ratio of Sr : Ti : M : Sb = $1.00 : 1 - x - y : x : y$. The mixture was calcined at 1173 K for 1 h in an alumina crucible, followed by calcination at 1273 K for 10 h in air. The obtained $SrTiO_3$:M(x%),Sb(y%) (M = Ir, Rh, Ru, Cr, Mn, Fe, Co, Ni), $SrCl_2 \cdot 6H_2O$ (Fujifilm Wako Pure Chemicals; 99%), and Al_2O_3 (Kanto Chemical; 99.0%) were mixed in an alumina mortar in a $1 : 10 : z$ atomic ratio to Ti. The mixture was heated in air at 1373 K for 10 h in an alumina crucible as the flux treatment. It is reported that Al^{3+} is doped also from an alumina crucible during the flux treatment.[34] Therefore, the samples after the flux treatment were described as $SrTiO_3$:M,Sb,Al (M = Ir, Rh, Ru, Cr, Mn, Fe, Co, Ni) even without Al_2O_3 addition. A flowchart of the preparation of the photocatalysts is provided in the ESI (Fig. S1†). The resulting powder was washed with water to remove the flux reagent.

$RhCrO_x$,[12,35,36] Rh_2O_3, Cr_2O_3, IrO_2, RuO_2, and CoO_x cocatalysts were loaded on the samples by an impregnation method. The obtained sample was dispersed in aqueous solutions dissolving $Rh(NO_3)_3$, $Cr(NO_3)_3$, $(NH_4)_2IrCl_6$, $RuCl_4$, and $Co(NO_3)_2$ in a porcelain crucible. The dispersion was heated in air to evaporate water following calcination in air at 623 K for 1 h for loading of $RhCrO_x$, Rh_2O_3, and Cr_2O_3 and at 673 K for 2 h for loading of IrO_2, RuO_2, and CoO_x. Rh and CrO_x cocatalysts[37,38] were also loaded *in situ* by a photodeposition method using aqueous solutions of $Rh(NO_3)_3$ and $Cr(NO_3)_3$.

Characterization

The crystal phase of the obtained sample was confirmed by X-ray diffraction (XRD; Rigaku; MiniFlex600) using Cu Kα radiation. Diffuse reflectance spectra were measured using a UV-Vis-NIR spectrometer (JASCO; UbeatV-570) equipped with an integrating sphere and were converted to a K–M function by the Kubelka–Munk method. The chemical composition of the sample was analyzed using an X-ray fluorescence spectrometer (XRF; Rigaku; NEXDE). The morphology and particle size of the sample were observed using a scanning electron microscope (SEM; JEOL; JSM-6700F).

Photocatalytic activity

Photocatalytic water splitting was carried out using a top-irradiation reaction cell with a Pyrex window connected to a gas-tight circulation system. A 300 W Xe-arc lamp (PerkinElmer; CERMAX PF300BF) attached to a long-pass filter (HOYA; Y44) and a solar simulator (ASAHI SPECTRA, HAL-320, 0.1 W cm^{-2}) were used as light sources. Irradiated areas using a 300 W Xe-arc lamp and a solar simulator were 33 and 16 cm^2, respectively. The evolved H_2 and O_2 were measured using an online gas chromatograph (Shimadzu; GC-8A, MS-5A column, TCD, Ar carrier). The apparent quantum yield (AQY) was calculated using the following equation.

$$\begin{aligned}\text{AQY (\%)} &= 100 \times [\text{the number of reacted holes}]/\\ &\quad [\text{the number of incident photons}] = 100\\ &\quad \times [\text{the number of evolved } O_2 \text{ molecules}]\\ &\quad \times 4/[\text{the number of incident photons}]\end{aligned}$$

The solar-to-hydrogen energy conversion efficiencies (STH) under full arc and visible light (λ > 440 nm) measured using a solar simulator were calculated using the following equations. Powers of a solar simulator were 0.1 W cm^{-2}.

$$\begin{aligned}\text{STH (\%)} &= (100 \times ([\Delta G^{\circ}(H_2O)/\text{J mol}^{-1}]\\ &\quad \times [\text{rate of } H_2 \text{ evolution/mol h}^{-1}])/([3600/\text{s h}^{-1}]\\ &\quad \times [\text{solar energy/W cm}^{-2}] \times [\text{irradiation area/cm}^2])\\ &= (100 \times 237\,000 \times [\text{rate of } H_2 \text{ evolution/mol h}^{-1}])/\\ &\quad (3600 \times 0.1 \times 16)\end{aligned}$$

Results and discussion

Characterization and water splitting over $SrTiO_3$:Ir,Sb,Al photocatalysts prepared by SSR followed by flux treatment in an alumina crucible

X-ray diffraction patterns of SSR-prepared $SrTiO_3$ and $SrTiO_3$:Ir(x%),Sb(y%) (x = 0.001–0.3, y = 0.002–0.6) with and without

the flux treatment in an alumina crucible were measured. A single phase of $SrTiO_3$ was obtained for all samples before and after the flux treatment without any impurities of Ir and Sb species. As previously reported, it was considered that Ir and Sb ions were substituted for Ti sites in $SrTiO_3$, judging from the ionic radii; Ti^{4+}: 0.605 Å, Ir^{3+}: 0.68 Å, Ir^{4+}: 0.625 Å, Sb^{5+}: 0.60 Å for 6 coordination. Peak shifts between non-doped $SrTiO_3$ and $SrTiO_3$:Ir(x%),Sb(y%) were not observed, due to the doping amounts of Ir and Sb being very small and/or the ionic radii of Ir and Sb ions being larger and smaller than that of a Ti ion, respectively. The Raman spectra of SSR-prepared $SrTiO_3$:Ir(x%),Sb(2x%),Al (x = 0–0.3) with the flux treatment were also measured (Fig. S2†). New Raman bands around 800 cm^{-1} were clearly observed with an increase in doping amounts of Ir and Sb although they were not observed for the non-doped sample. It has been reported that the Raman band at around 800 cm^{-1} appears when different elements are substituted for the B-site of ABO_3 with the perovskite structure due to the formation of an ordered distribution at the B-site.[39] These XRD patterns and Raman spectra indicated that Ir and Sb ions were successfully doped at the Ti sites of $SrTiO_3$. Next, XRF analysis of $SrTiO_3$:Ir(x%),Sb(2x%) (x = 0.025–0.3) was carried out to confirm the amounts of Ir and Sb doped in the photocatalyst (Table S1†). The Ir and Sb ions of x = 0.025 could not be detected due to the doping amounts being very small. The amounts of Ir and Sb in the samples with x = 0.05–0.3 before the flux treatment were almost the same as those after the flux treatment. It is suggested that dopants of Ir and Sb were not lost to a flux reagent.

Fig. 1 shows the diffuse reflectance spectra of $SrTiO_3$:Ir(x%),Sb(2x%) (x = 0–0.3) before and after the flux treatment. The absorption in the visible light region increased upon an increase in the doping amount of Ir. The absorption in the range of visible light negligibly changed on the sample with x = 0.001–0.01% after the flux treatment. In contrast to it, the absorption of the samples with x = 0.05–0.3% greatly increased after the flux treatment. The increase in the visible light absorption region would mainly be due to the increase in the particle size as shown in Fig. 2. It was confirmed by previous reports that absorptions at around 500–800 nm and 400–

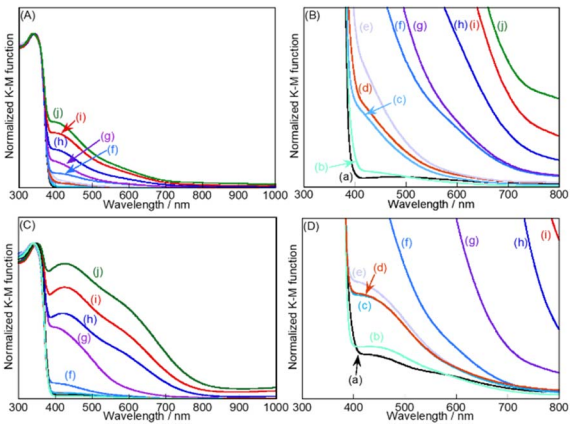

Fig. 1 Diffuse reflectance spectra of SSR-prepared $SrTiO_3$:Ir(x%),Sb(2x%) (A and B) without and (C and D) with the flux treatment without Al_2O_3 addition. Samples were doped with (a) x = 0, (b) x = 0.001, (c) x = 0.008, (d) x = 0.009, (e) x = 0.01, (f) x = 0.025, (g) x = 0.05, (h) x = 0.1, (i) x = 0.2, and (j) x = 0.3. (A and C) Full and (B and D) enlarged scales.

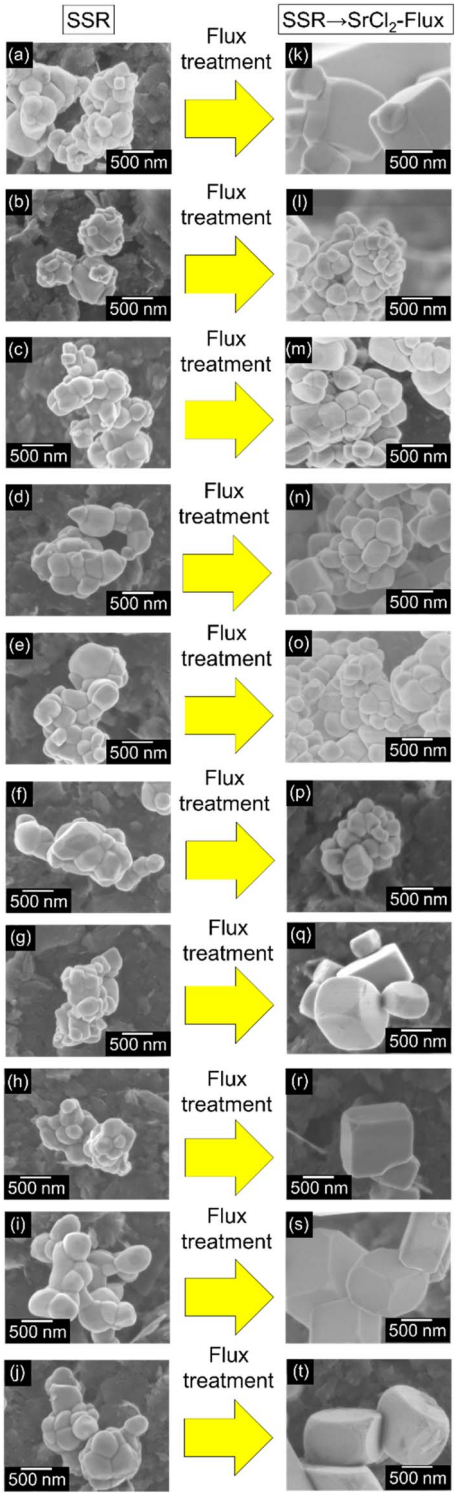

Fig. 2 SEM images of SSR-prepared $SrTiO_3$:Ir(x%),Sb(2x%) (a–j) without and (k–t) with the flux treatment in an alumina crucible. Samples were doped with (a and k) x = 0, (b and l) x = 0.001, (c and m) x = 0.008, (d and n) x = 0.009, (e and o) x = 0.01, (f and p) x = 0.025, (g and q) x = 0.05, (h and r) x = 0.1, (i and s) x = 0.2, and (j and t) x = 0.3.

450 nm were assigned to transitions from Ir^{3+} ions to a conduction band, and a valence band to Ir^{4+} ions, respectively.[29,40]

The morphologies of $SrTiO_3$:Ir(x%),Sb($2x$%) particles before and after the flux treatment in an alumina crucible were observed by scanning electron microscopy measurements as shown in Fig. 2. The flux-treated samples had a cubic-like shape with the specific facets whereas non-flux-treated samples were sphere-like particles with no specific facet. It was previously reported that the flux treatment contributed to the formation of truncated particles.[31,34,41] The flux-treated particles of $x = 0.001$–0.025 were mainly 0.1–0.5 μm whereas large particles of sub-micrometer order were partially observed. In contrast to them, those of $x = 0$, 0.05–0.3% were mainly 0.3–10 μm. It was found that small amounts of Ir and Sb doping suppressed crystal growth.

Photocatalytic overall water splitting over $RhCrO_x$-loaded $SrTiO_3$:Ir(x%),Sb($2x$%) under visible light irradiation was carried out as shown in Table 1. Efficient water splitting proceeded over Ir,Sb-codoped samples with the flux treatment compared with a non-doped sample. However, the Ir,Sb-codoped sample without the flux treatment showed negligible activity, indicating that the flux treatment was essential for efficient water splitting. It has been reported by Ham and Domen that the photocatalytic activity for water splitting was greatly improved by usage of an alumina crucible but not usage of an Y_2O_3 crucible for the flux treatment.[31] Al was doped into a $SrTiO_3$ photocatalyst from the alumina crucible during the flux treatment. Therefore, Al is also doped into the Ir,Sb co-doped $SrTiO_3$ photocatalyst in the present study even without intentional Al_2O_3 addition. The Al doping by the flux treatment using an alumina crucible actually affects water splitting in the present Ir,Sb co-doped $SrTiO_3$ photocatalyst. The flux treatment accompanied by Al doping to the sample doped with the small amounts of Ir and Sb contributed to suppression of particle growth and formation of the specific facet which worked as the active sites for water splitting and efficient charge separation of photo-generated electrons and holes.[34] The activity increased with an increase in the doping amount up to $x = 0.009\%$ (Table 1, entries 1–4 and 7), which was due to an increase in visible light absorption by formation of an impurity level of an Ir dopant. In contrast to it, the activity of the samples decreased with a further increase in the doping amounts of Ir and Sb (Table 1, entries 7 and 9–14), which was due to an increase in recombination centers by dopants and formation of large particles as shown in Fig. 2.

Table 1 Photocatalytic water splitting over $RhCrO_x$-loaded $SrTiO_3$:Ir,Sb under visible light irradiation[a]

Entry	Dopant (mol% to Ti)	$SrCl_2$-flux treatment	Water splitting activity/μmol h^{-1}	
			H_2	O_2
1	None	Yes	0.14	0.05
2	Sb(0.018%)	Yes	0.17	0.07
3	Ir(0.001%),Sb(0.002%)	Yes	4.2	1.9
4	Ir(0.008%),Sb(0.016%)	Yes	33	16
5	Ir(0.009%)	Yes	20	9.4
6	Ir(0.009%),Sb(0.009%)	Yes	29	14
7	Ir(0.009%),Sb(0.018%)	Yes	41	21
8	Ir(0.009%),Sb(0.027%)	Yes	16	7.8
9	Ir(0.01%),Sb(0.02%)	Yes	36	15
10	Ir(0.025%),Sb(0.05%)	Yes	21	11
11	Ir(0.05%),Sb(0.1%)	Yes	8.2	4.0
12	Ir(0.1%),Sb(0.2%)	Yes	3.1	1.4
13	Ir(0.2%),Sb(0.4%)	Yes	1.1	0.5
14	Ir(0.3%),Sb(0.6%)	Yes	0.15	0.08
15	None	No	0.01	0.005
16	Ir(0.009%),Sb(0.018%)	No	0.02	0.01

[a] Photocatalyst: 0.2 g, cocat.: $RhCrO_x$ (Rh 0.1 mol%, Cr 0.1 mol%) impregnation, reactant solution: pure water (120 mL), light source: a 300 W Xe lamp ($\lambda > 440$ nm), cell: a top-irradiation cell with a Pyrex window, system: a gas-tight circulation system.

Next, the effect of the codoping amount of Sb on photocatalytic water splitting over $SrTiO_3$:Ir(0.009%),Sb(y%),Al under visible light irradiation was examined. The activity was increased by Sb codoping up to 0.018% (Table 1, entries 5–7) because of charge compensation by Sb doping in the oxidation number of Ir. In contrast, the activity of the sample doped with a large amount of Sb decreased (Table 1, entry 8). Many large particles of the sample were observed by SEM (Fig. S3(g)†), which is the main factor in the low activity. It was clarified that 0.009% of Ir and 0.018% of Sb were the optimum doping amounts. We have reported that stoichiometric codoping of Sb^{5+} ions was not enough for charge compensation to doped transition metal ions such as Rh and Cr.[28,42–44] Electron spin resonance (ESR) measurements of TiO_2:Rh,Sb and $SrTiO_3$:Rh,Sb revealed that the ESR signals related to Rh^{4+} ions were considerably suppressed by Sb codoped with more than the stoichiometric ratio, 1 : 1.[43,44] Therefore, an excess amount of Sb doping (Ir : Sb = 1 : 2) was necessary for a high enough charge compensation that had a positive effect on water splitting over the $SrTiO_3$:Ir,Sb,Al photocatalyst.

Effect of intentional Al_2O_3 addition for the flux treatment on photocatalytic water splitting

Doping of a cation with a lower oxidation number than the parent cation into a host material is sometimes effective for the improvement of photocatalytic activity.[45,46] It has been reported that doping of an Al^{3+} ion to Ti^{4+} sites in the $SrTiO_3$ host plays an important role in suppressing Ti^{3+} ions which work as recombination centers for photogenerated carriers, and decreasing the n-type semiconductor character of $SrTiO_3$.[47,48] In addition, Al_2O_3 addition to the flux treatment produces fine particles of *ca.* 300 nm. Therefore, the effect of intentional Al_2O_3 addition in the flux reagent to the $SrTiO_3$:Ir(0.009%),Sb(0.018%),Al photocatalyst on water splitting under visible light irradiation was investigated. No impurities of Ir, Sb, and Al species, and no peak shifts were observed in the X-ray diffraction patterns of the samples prepared by the flux treatment with various amounts of Al_2O_3 (0–3%), suggesting that Al ions were successfully doped to Ti^{4+} sites in $SrTiO_3$ more or less.

The effect of an amount of Al_2O_3 addition in the flux for the preparation of $SrTiO_3$:Ir(0.009%),Sb(0.018%),Al on

photocatalytic water splitting under visible light irradiation was investigated (Table S2†). All samples prepared with Al_2O_3 addition showed higher activity than that without Al_2O_3 addition. The optimum amount of added Al^{3+} was 1–2 mol%.

Effect of loading of cocatalysts on photocatalytic water splitting

The activity for photocatalytic water splitting greatly depends on cocatalysts as active sites. Therefore, the effect of loading with various cocatalysts on water splitting over $SrTiO_3$:Ir(0.009%),Sb(0.018%),Al prepared with Al_2O_3 (1%) addition in the flux was examined. Photocatalytic water splitting proceeded with a reasonable activity when $RhCrO_x$ (H_2: 62 μmol h^{-1}, O_2: 30 μmol h^{-1}) and Rh_2O_3 (H_2: 12 μmol h^{-1}, O_2: 5.6 μmol h^{-1}) cocatalysts were loaded (Table S3†). The $RhCrO_x$ cocatalyst was more effective among these cocatalysts. It was previously reported that $RhCrO_x$ promoted the H_2 evolution reaction and suppressed a backward reaction from evolved H_2 and O_2 to form water and photoreduction of O_2.[49] We carried out photodeposition of CrO_x and Rh cocatalysts on a $SrTiO_3$:Ir,Sb,Al photocatalyst for water splitting under visible light irradiation. The photodeposition method did not give a higher activity (H_2: 41 μmol h^{-1}, O_2: 18 μmol h^{-1}) than an impregnation method (H_2: 62 μmol h^{-1}, O_2: 30 μmol h^{-1}) with the same loading amount. The impregnated cocatalysts would dissolve and re-photodeposit during irradiation, resulting in the impregnated cocatalyst becoming similar to the photodeposited one. The optimum loading amount of the $RhCrO_x$ cocatalyst was 0.1 mol% (Table S3, entries 2–5†). The photocatalyst optimized for doping amounts, Al_2O_3 addition in a flux treatment, and the cocatalyst split water into H_2 and O_2 in a stoichiometric amount under visible light irradiation (Fig. S4†).

For an Al-doped $SrTiO_3$ photocatalyst, the facets of (100) as a reduction site and (110) as an oxidation site were exposed on a particle, promoting H_2 and O_2 evolution from water separately.[34] Therefore, we observed reductively and oxidatively photodeposited Ag and PbO_2, respectively, under visible light irradiation (λ > 440 nm) on $SrTiO_3$:Ir(0.009%),Sb(0.018%),Al particles prepared by Al_2O_3 addition in the flux by SEM as shown in Fig. 3. The SEM images showed that Ag and PbO_2 particles were deposited on a reductive facet of (100) and an oxidative facet of (110), respectively. This indicated that photogenerated carriers separated to the reductive and oxidative facets on the photocatalyst surface.

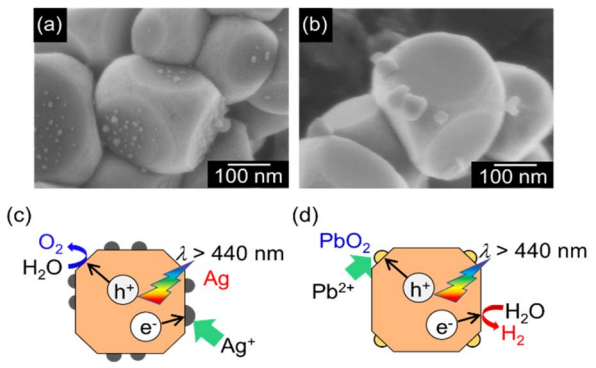

Fig. 3 SEM images of (a) Ag (3 wt%)- and (b) PbO_2 (5 wt%)-deposited $SrTiO_3$:Ir(0.009%),Sb(0.018%),Al prepared by the flux treatment with Al_2O_3 (1%) addition after SSR. Ag and PbO_2 were loaded by a photodeposition method under visible light irradiation (λ > 440 nm). The mechanism of photo-deposition of (c) Ag and (d) PbO_2 on the photocatalyst.

Mechanism of water splitting under visible light irradiation over a $RhCrO_x$-loaded $SrTiO_3$:Ir,Sb,Al photocatalyst

The action spectra of $RhCrO_x$ (0.1 mol%)-loaded $SrTiO_3$:Ir(0.009%),Sb(0.018%),Al prepared with Al_2O_3 (1%) addition in

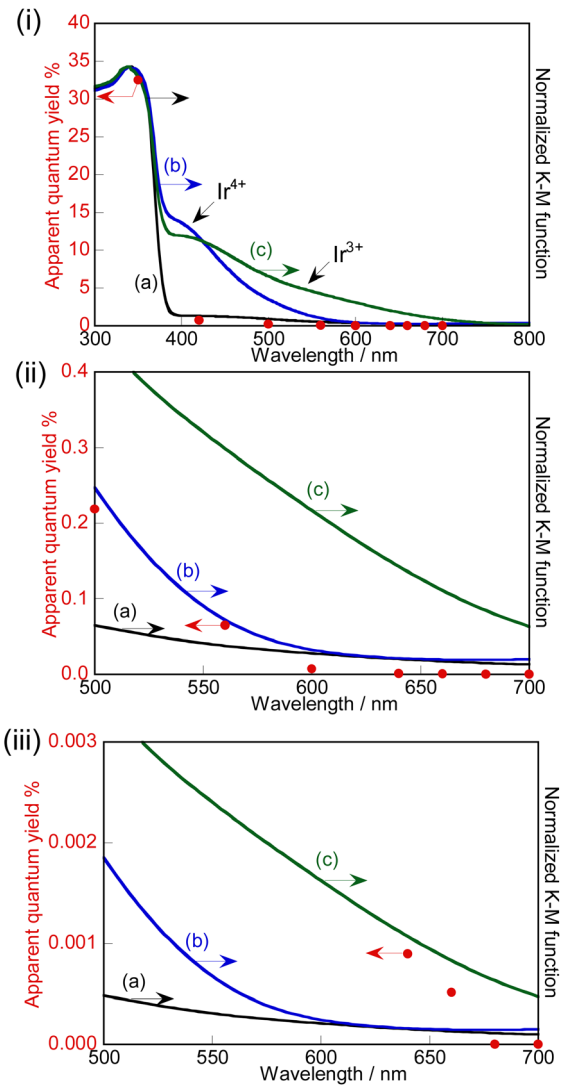

Fig. 4 Action spectrum of photocatalytic water splitting over $RhCrO_x$(0.1 mol%)-loaded $SrTiO_3$:Ir(0.009%),Sb(0.018%),Al prepared by the flux treatment with Al_2O_3 (1%) addition after SSR and diffuse reflectance spectra of (a) $SrTiO_3$:Ir(0.009%),Sb(0.018%) prepared by the flux treatment with Al_2O_3 (1%) addition after SSR, (b) $SrTiO_3$:Ir(0.2%), and (c) H_2-reduced (673 K, 1 h) $SrTiO_3$:Ir(0.2%). (ii) An enlarged scale of (i); (iii) an enlarged scale of (ii). Photocatalyst: 0.5 g, cocat.: $RhCrO_x$ (impregnation), reactant solution: pure water (120 mL), light source: a 300 W Xe lamp with band-pass filters, cell: a top-irradiation cell with a Pyrex window, system: a gas-tight circulation system.

the flux for photocatalytic water splitting are shown in Fig. 4. The photocatalyst responded up to 660 nm which is the longest wavelength among the previously reported visible-light-driven single particulate photocatalysts being active for water splitting. Stoichiometric O_2 evolution was also observed up to 660 nm. The profiles of action spectra and the onset were similar to the action spectra of Ir-doped $SrTiO_3$ for the photoanodic properties for oxidation of water.[40,50]

We discuss the photoexcitation mechanism for water splitting on a $SrTiO_3$:Ir(0.009%),Sb(0.018%),Al photocatalyst based on an action spectrum and diffuse reflectance spectra. The absorption edge of a non-H_2-treated $SrTiO_3$:Ir(0.2%) was around 580 nm, indicating that the absorption was due to photoexcitation from a valence band to the impurity level consisting of Ir^{4+} ions as shown in Fig. 4(i). The absorption edge was redshifted to around 750 nm by H_2 reduction, indicating that the photoexcitation was due to transition from an impurity level consisting of Ir^{3+} ions to a conduction band.[29,40]

The photocatalyst activity was observed by utilizing absorptions related to Ir^{4+} ($\lambda \leq$ *ca.* 560 nm) and Ir^{3+} ($\lambda \leq$ *ca.* 660 nm) ions. In the one-step photoexcitation process as shown in Fig. 5(i), the conduction band level and holes transiently photogenerated in the impurity level consisting of Ir^{3+} ions thermodynamically satisfy the reduction and oxidation of water, with water splitting being able to proceed. However, the activity by photoexcitation at wavelengths longer than 600 nm was low due to poor migration of holes in the low concentration of an impurity level and small potential difference between the impurity level consisting of Ir^{3+} and water oxidation as shown in Fig. 4(iii). In contrast to it, AQY greatly increased with simultaneous photoexcitation ($\lambda \leq$ *ca.* 560 nm) of both absorption bands related to Ir^{3+} and Ir^{4+} ions as shown in Fig. 4(ii). In this scheme, Ir^{4+} ions are reduced to Ir^{3+} ions by photoexcitation from a valence band to Ir^{4+} ions as shown in Fig. 5(ii), which is a similar trend to the case of a Rh-doped $SrTiO_3$ photocatalyst,[23] and subsequently the electrons at the formed Ir^{3+} ions are excited to a conduction band. Then, Ir^{3+} ions return to Ir^{4+} ions after photoexcitation from Ir^{3+} ions. This results in e^- and h^+ being photogenerated in the conduction and valence bands of $SrTiO_3$ through this two-step photoexcitation, respectively. Therefore, migration of photogenerated carriers in the conduction and valence bands becomes smooth compared with that *via* the one-step photoexcitation process, resulting in the high activity. Here, the redox in Ir^{4+}/Ir^{3+} occurs in one Ir cation, but not Z-scheme electron flow. The maximum AQY was estimated to be 0.73% at 420 nm.

Photocatalytic solar water splitting over $RhCrO_x$-loaded $SrTiO_3$:Ir(0.009%),Sb(0.018%),Al prepared with Al_2O_3 (1%) addition in the flux proceeded as shown in Fig. 6, giving 0.33% STH. H_2 and O_2 stoichiometrically evolved for 20 h. The

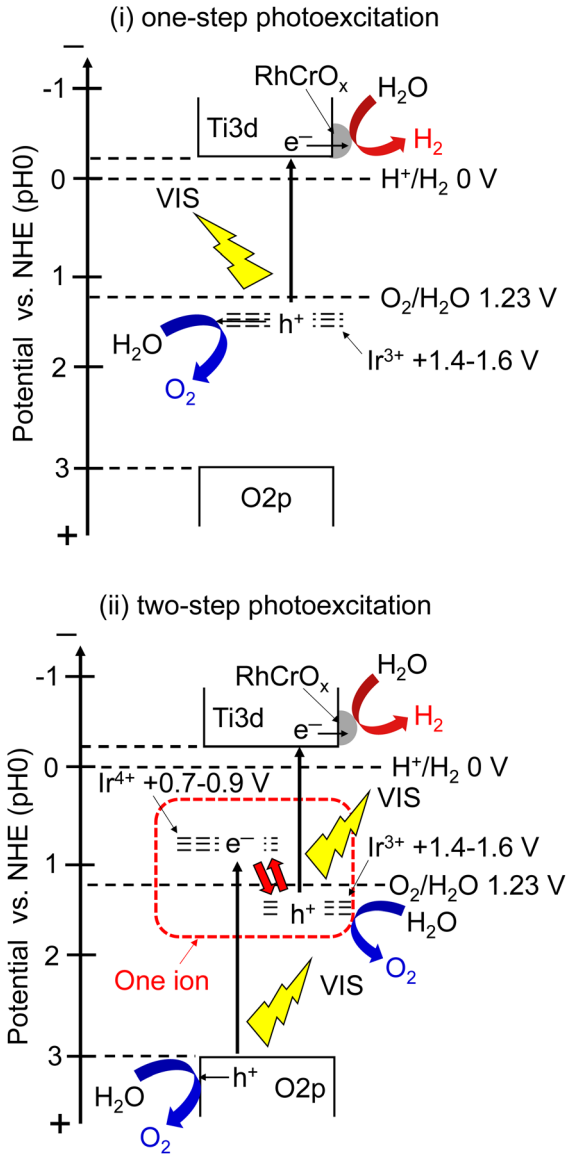

Fig. 5 Proposed mechanism of water splitting over a $SrTiO_3$:Ir,Sb,Al photocatalyst under visible light irradiation. (i) One-step photoexcitation, (ii) two-step photoexcitation.

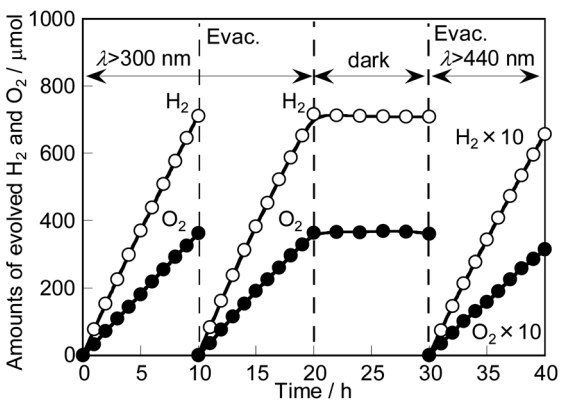

Fig. 6 Photocatalytic water splitting over $RhCrO_x$-loaded $SrTiO_3$:Ir(0.009%),Sb(0.018%),Al prepared by the flux treatment with Al_2O_3 (1%) addition after SSR under simulated sunlight irradiation. Photocatalyst: 0.5 g, cocat.: $RhCrO_x$ (Rh 0.1 mol%, Cr 0.1 mol%) impregnation, reactant solution: pure water (120 mL), light source: a solar simulator (AM 1.5G), irradiation area: 16 cm^2, system: a gas-tight circulation system.

amounts of H_2 and O_2 did not decrease under dark conditions, suggesting that the backward reaction of the formation of H_2O hardly occurred. In addition, 0.030% STH was also obtained by using only visible light ($\lambda > 440$ nm) from a solar simulator. This is currently the highest value for water splitting with a single particulate photocatalyst compared with previously reported visible-light-driven photocatalysts. The turnover numbers estimated from electrons used for evolved H_2 (65.6 μmol) for 10 h under visible light ($\lambda > 440$ nm) from a solar simulator to the mole number of an Ir dopant (0.245 μmol) of $SrTiO_3$:Ir,Sb,Al and a $RhCrO_x$ cocatalyst (2.73 μmol) were about 536 and 48.1, respectively, indicating that this reaction proceeded photocatalytically.

Water splitting over $RhCrO_x$-loaded various transition metal-doped $SrTiO_3$:Al photocatalysts

To expand the doping species of the transition metal, water splitting over various transition metal-doped $SrTiO_3$:Al photocatalysts prepared with Al_2O_3 (1%) addition for the flux treatment was investigated as shown in Table 2. We would have investigated the XPS and XRF of $SrTiO_3$:Ir,Sb,Al after flux treatment with Al_2O_3 addition. However, the Al signal was not clearly detected due to a small amount of doped Al ions in the photocatalyst. Therefore, we could not determine the quantity of doped Al here. Rh, Ru, and Cr-doped samples showed high activity for water splitting under visible light as well as with an Ir dopant. It was notable that solar water splitting proceeded under visible light ($\lambda > 440$ nm) over all samples (Table S4†). We have preliminarily reported that the flux-treated $SrTiO_3$:Al doped with small amounts of Rh, Ru and Cr was active for photocatalytic water splitting.[51–53] Recently, single particulate $KTaO_3$:Ir,A (A = Ca, Sr, Ba, La), $SrTiO_3$:Cr,La,Al, and $KTaO_3$:Ru,La oxide photocatalysts for water splitting under visible light irradiation have been developed by doping small amounts of transition metal dopants, and loading with Rh–Cr-based cocatalysts,[54–56] this being similar to our strategy.[51–53] Our $SrTiO_3$:Ir,Sb,Al and $SrTiO_3$:Ru,Sb,Al showed much higher activity than the $KTaO_3$:Ir,A and $KTaO_3$:Ru,La. In our present study, the activities of $SrTiO_3$:Cr,Al and $SrTiO_3$:Ru,Sb,Al were improved by optimization of the doping amount and the preparation conditions. The Rh and Sb-codoped, Ru and Sb-codoped, and Cr-doped photocatalysts responded to 570, 600 and 660 nm, respectively. Among the samples, $SrTiO_3$:Ir(0.009%),Sb(0.018%),Al showed the highest activity. Thus, the development of various transition metal-doped photocatalysts as single particulate photocatalysts for highly efficient water splitting was successful with small amounts of dopants, the flux treatment, and $RhCrO_x$ cocatalyst loading.

Table 2 Water splitting over $RhCrO_x$-loaded various transition metal-doped $SrTiO_3$:Al photocatalysts prepared by the flux treatment with Al_2O_3(1%) addition after SSR under visible light irradiation[a]

Dopant (mol% to Ti)	Responsive wavelength/nm	Water splitting activity/μmol h^{-1}	
		H_2	O_2
Ir(0.009%),Sb(0.018%),Al	660	62	30
Rh(0.02%),Sb(0.04%),Al	570	56	28
Ru(0.03%),Sb(0.06%),Al	600	54	27
Cr(0.01%),Al	660	21	12
Mn(0.01%),Al	—	0.81	0.43
Fe(0.01%),Al	—	0.29	0.15
Co(0.01%),Al	—	1.5	0.72
Ni(0.01%),Al	—	0.77	0.38

[a] Photocatalyst: 0.2 g, cocatalyst: $RhCrO_x$ (Rh 0.1 mol%, Cr 0.1 mol%), reactant solution: pure water (120 mL), light source: a 300 W Xe lamp ($\lambda > 440$ nm), cell: a top-irradiation cell with a Pyrex window, system: a gas-tight circulation system.

Conclusions

Strategies of a small doping amount of transition metals to suppress recombination between photogenerated electrons and holes, flux treatment with Al_2O_3 addition for formation of homogeneous fine particles with exposed reductive and oxidative facets, and loading of a $RhCrO_x$ cocatalyst as an active site were effective for the development of a highly efficient doping photocatalyst for water splitting under visible light. Efficient photocatalytic water splitting under visible light irradiation over $RhCrO_x$-loaded $SrTiO_3$:Ir,Sb,Al as a single particulate metal oxide photocatalyst was achieved by the strategy. The high activity was obtained by the flux treatment with Al_2O_3 addition to the SSR-prepared samples, doping of small amounts of Ir and Sb, and loading of a $RhCrO_x$ cocatalyst. The optimized photocatalyst responded to 660 nm that is currently the highest value for water splitting with a single particulate photocatalyst compared with previously reported visible-light-driven photocatalysts. The maximum AQY reached 0.73% at 420 nm. Solar water splitting under full arc and visible light ($\lambda > 440$ nm) proceeded, giving 0.33% and 0.030% STHs ($\lambda > 440$ nm), respectively. It is proposed that photocatalytic water splitting under visible light irradiation over $RhCrO_x$-loaded $SrTiO_3$:Ir,Sb,Al proceeded *via* two-step photoexcitation utilizing subsequent absorptions from a valence band to Ir^{4+} ions and from Ir^{3+} ions to a conduction band in one Ir cation based on the results of diffuse reflectance spectra and an action spectrum. Additionally, various transition metal doped-$SrTiO_3$:Al photocatalysts were developed for water splitting as a single particulate photocatalyst in the same manner as the Ir,Sb-codoped sample. In particular, Ru(0.03%) and Sb(0.06%)-codoped and Cr(0.01%)-doped samples showed activity for water splitting under visible light up to 600 and 660 nm, respectively. These strategies are expected to be applied for doping other photocatalysts for water splitting.

Data availability

All data are available in the main manuscript and the ESI.†

Author contributions

K. K.: methodology, investigation, visualization, and writing – original draft. Y. U., H. K.: methodology, investigation, and

visualization. K. W., S. Y., Y. Y.: methodology and writing – review and editing. A. K.: conceptualization, supervision and writing – reviewing and editing.

Conflicts of interest

There are no conflicts to declare.

Acknowledgements

This work was supported by JSPS KAKENHI, Grant Numbers 17H06433 and 23H00248 in Scientific Research on "Innovative Areas for Light-Energy Conversion (I^4LEC)", 17H01217 and 22K14770, and the Tokyo University of Science Grant for President's Research Promotion.

References

1 F. E. Osterloh, *Chem. Mater.*, 2008, **20**, 35–54.
2 A. Kudo and Y. Miseki, *Chem. Soc. Rev.*, 2009, **38**, 253–278.
3 R. Abe, *J. Photochem. Photobiol., C*, 2010, **11**, 179–209.
4 T. Hisatomi, J. Kubota and K. Domen, *Chem. Soc. Rev.*, 2014, **43**, 7520–7535.
5 H. Nishiyama, T. Yamada, M. Nakabayashi, Y. Maehara, M. Yamaguchi, Y. Kuromiya, H. Tokudome, S. Akiyama, T. Watanabe, R. Narushima, S. Okunaka, N. Shibata, T. Takata, T. Hisatomi and K. Domen, *Nature*, 2021, **598**, 304–307.
6 S. Nandy, T. Hisatomi, T. Takata, T. Setoyama and K. Domen, *J. Mater. Chem. A*, 2023, **11**, 20470–20479.
7 A. Kudo, H. Kato and I. Tsuji, *Chem. Lett.*, 2004, **33**, 1534–1539.
8 K. Maeda, *ACS Catal.*, 2013, **3**, 1486–1503.
9 Y. Wang, H. Suzuki, J. Xie, O. Tomita, D. J. Martin, M. Higashi, D. Kong, R. Abe and J. Tang, *Chem. Rev.*, 2018, **118**, 5201–5241.
10 Y. Ma, L. Lin, T. Takata, T. Hisatomi and K. Domen, *Phys. Chem. Chem. Phys.*, 2023, **25**, 6586–6601.
11 K. Maeda, T. Takata, M. Hara, N. Saito, Y. Inoue, H. Kobayashi and K. Domen, *J. Am. Chem. Soc.*, 2005, **127**, 8286–8287.
12 K. Maeda, K. Teramura, D. Lu, T. Takata, N. Saito, Y. Inoue and K. Domen, *Nature*, 2006, **440**, 295.
13 Y. Lee, H. Terashima, Y. Shimodaira, K. Teramura, M. Hara, H. Kobayashi, K. Domen and M. Yashima, *J. Phys. Chem. C*, 2007, **111**, 1042–1048.
14 X. Wang, K. Maeda, Y. Lee and K. Domen, *Chem. Phys. Lett.*, 2008, **457**, 134–136.
15 Q. Wang, M. Nakabayashi, T. Hisatomi, S. Sun, S. Akiyama, Z. Wang, Z. Pan, X. Xiao, T. Watanabe, T. Yamada, N. Shibata, T. Takata and K. Domen, *Nat. Mater.*, 2019, **18**, 827–832.
16 Z. Wang, Y. Inoue, T. Hisatomi, R. Ishikawa, Q. Wang, T. Takata, S. Chen, N. Shibata, Y. Ikuhara and K. Domen, *Nat. Catal.*, 2018, **1**, 756–763.
17 K. Maeda, D. Lu and K. Domen, *Chem.–Eur. J.*, 2013, **19**, 4986–4991.
18 C. Pan, T. Takata and K. Domen, *Chem.–Eur. J.*, 2016, **22**, 1854–1862.
19 H. Li, J. Xiao, J. J. M. Vequizo, T. Hisatomi, M. Nakabayashi, Z. Pan, N. Shibata, A. Yamakata, T. Takata and K. Domen, *ACS Catal.*, 2022, **12**, 10179–10185.
20 S. Nishimae, J. J. M. Vequizo, Y. Inoue, A. Yamakata, M. Nakabayashi, T. Higashi and K. Domen, *J. Mater. Chem. A*, 2023, **11**, 6299–6310.
21 K. Chen, J. Xiao, J. J. M. Vequizo, T. Hisatomi, Y. Ma, M. Nakabayashi, T. Takata, A. Yamakata, N. Shibata and K. Domen, *J. Am. Chem. Soc.*, 2023, **145**, 3839–3843.
22 Y. Sakata, T. Yamamoto, T. Okazaki, H. Imamura and S. Tsuchiya, *Chem. Lett.*, 1998, **27**, 1253–1254.
23 R. Konta, T. Ishii, H. Kato and A. Kudo, *J. Phys. Chem. B*, 2004, **108**, 8992–8995.
24 D. W. Hwang, H. G. Kim, J. S. Jang, S. W. Bae, S. M. Ji and J. S. Lee, *Catal. Today*, 2004, **93–95**, 845–850.
25 Y. Shimodaira, H. Kato, H. Kobayashi and A. Kudo, *Bull. Chem. Soc. Jpn.*, 2007, **80**, 885–893.
26 Y. Yamaguchi and A. Kudo, *Front. Energy*, 2021, **15**, 568–576.
27 S. Sun, T. Hisatomi, Q. Wang, S. Chen, G. Ma, J. Liu, S. Nandy, T. Minegishi, M. Katayama and K. Domen, *ACS Catal.*, 2018, **8**, 1690–1696.
28 R. Asai, H. Nemoto, Q. Jia, K. Saito, A. Iwase and A. Kudo, *Chem. Commun.*, 2014, **50**, 2543–2546.
29 S. Suzuki, H. Matsumoto, A. Iwase and A. Kudo, *Chem. Commun.*, 2018, **54**, 10606–10609.
30 A. Kudo, S. Yoshino, T. Tsuchiya, Y. Udagawa, Y. Takahashi, M. Yamaguchi, I. Ogasawara, H. Matsumoto and A. Iwase, *Faraday Discuss.*, 2019, **215**, 313–328.
31 Y. Ham, T. Hisatomi, Y. Goto, Y. Moriya, Y. Sakata, A. Yamakata, J. Kubota and K. Domen, *J. Mater. Chem. A*, 2016, **4**, 3027–3033.
32 T. H. Chiang, H. Lyu, T. Hisatomi, Y. Goto, T. Takata, M. Katayama, T. Minegishi and K. Domen, *ACS Catal.*, 2018, **8**, 2782–2788.
33 Y. Goto, T. Hisatomi, Q. Wang, T. Higashi, K. Ishikiriyama, T. Maeda, Y. Sakata, S. Okunaka, H. Tokudome, M. Katayama, S. Akiyama, H. Nishiyama, Y. Inoue, T. Takewaki, T. Setoyama, T. Minegishi, T. Takata, T. Yamada and K. Domen, *Joule*, 2018, **2**, 509–520.
34 T. Takata, J. Jiang, Y. Sakata, M. Nakabayashi, N. Shibata, V. Nandal, K. Seki, T. Hisatomi and K. Domen, *Nature*, 2020, **581**, 411–414.
35 K. Maeda, K. Teramura, D. Lu, T. Takata, N. Saito, Y. Inoue and K. Domen, *J. Phys. Chem. B*, 2006, **110**, 13753–13758.
36 K. Maeda, K. Teramura, N. Saito, Y. Inoue and K. Domen, *J. Catal.*, 2006, **243**, 303–308.
37 K. Maeda, K. Teramura, D. Lu, N. Saito, Y. Inoue and K. Domen, *Angew. Chem., Int. Ed.*, 2006, **45**, 7806–7809.
38 K. Maeda, K. Teramura, D. Lu, N. Saito, Y. Inoue and K. Domen, *J. Phys. Chem. C*, 2007, **111**, 7554–7560.
39 H. Zheng, I. M. Reaney, G. D. C. Csete de Györgyfalva, R. Ubic, J. Yarwood, M. P. Seabra and V. M. Ferreira, *J. Mater. Res.*, 2004, **19**, 488–495.
40 S. Kawasaki, R. Takahashi, K. Akagi, J. Yoshinobu, F. Komori, K. Horiba, H. Kumigashira, K. Iwashina,

A. Kudo and M. Lippmaa, *J. Phys. Chem. C*, 2014, **118**, 20222–20228.
41 H. Kato, M. Kobayashi, M. Hara and M. Kakihana, *Catal. Sci. Technol.*, 2013, **3**, 1733–1738.
42 H. Kato and A. Kudo, *J. Phys. Chem. B*, 2002, **106**, 5029–5034.
43 R. Niishiro, R. Konta, H. Kato, W.-J. Chun, K. Asakura and A. Kudo, *J. Phys. Chem. C*, 2007, **111**, 17420–17426.
44 R. Niishiro, S. Tanaka and A. Kudo, *Appl. Catal., B*, 2014, **150–151**, 187–196.
45 T. Ishihara, H. Nishiguchi, K. Fukamachi and Y. Takita, *J. Phys. Chem. B*, 1999, **103**, 1–3.
46 T. Takata and K. Domen, *J. Phys. Chem. C*, 2009, **113**, 19386–19388.
47 D. H. K. Murthy, V. Nandal, A. Furube, K. Seki, R. Katoh, H. Lyu, T. Hisatomi, K. Domen and H. Matsuzaki, *Adv. Energy Mater.*, 2023, **13**, 2302064.
48 R. Li, T. Takata, B. Zhang, C. Feng, Q. Wu, C. Cui, Z. Zhang, K. Domen and Y. Li, *Angew. Chem., Int. Ed.*, 2023, **62**, e202313537.
49 K. Maeda, K. Teramura, H. Masuda, T. Takata, N. Saito, Y. Inoue and K. Domen, *J. Phys. Chem. B*, 2006, **110**, 13107–13112.
50 S. Kawasaki, R. Takahashi, T. Yamamoto, M. Kobayashi, H. Kumigashira, J. Yoshinobu, F. Komori, A. Kudo and M. Lippmaa, *Nat. Commun.*, 2016, **7**, 11818.
51 K. Kaiya, K. Watanabe, S. Yoshino, Y. Yamaguchi and A. Kudo, *Abstracts of Papers (in Japanese), 126th CATSJ Meeting, Online, Japan*, 2020, p. P058.
52 K. Kaiya, Master thesis (in Japanese), Tokyo University of Science, Tokyo, Japan, 2021.
53 H. Kawamoto, Master thesis (in Japanese), Tokyo University of Science, Tokyo, Japan, 2022.
54 A. Iwase and H. Misono, *Chem. Commun.*, 2021, **57**, 10331–10334.
55 A. Iwase and H. Misono, *Energy Technol.*, 2023, **11**, 2200739.
56 Y. Qin, R. Xu, L. Ding, T. Wang, D. Guo, F. Fang and K. Chang, *J. Catal.*, 2024, **430**, 115317.